Energy exchange between coupled mechanical oscillators: linear regimes

Journal of Physics Communications

OPEN ACCESS

RECEIVED
25 June 2018

REVISED
30 August 2018

ACCEPTED FOR PUBLICATION
7 September 2018

PUBLISHED
19 September 2018

PAPER

Energy exchange between coupled mechanical oscillators: linear regimes

Damián H Zanette

Centro Atómico Bariloche and Instituto Balseiro, Comisión Nacional de Energía Atómica, Universidad Nacional de Cuyo. Consejo Nacional de Investigaciones Científicas y Técnicas. 8400 San Carlos de Bariloche, Río Negro, Argentina

E-mail: zanette@cab.cnea.gov.ar

Keywords: harmonic oscillators, micro-mechanical oscillators, nanomechanical oscillators

Abstract

Nonlinear mechanisms are frequently invoked to explain unexpected observations during processes of energy exchange in mechanical systems. However, whether the same phenomena could be observed in a purely linear system is seldom considered. In this paper, we revisit the problem of two linearly coupled, damped, harmonic oscillators, with emphasis on the dynamics of their mutual exchange of energy. A novel criterion is established to discern between two well-differentiated regimes of energy exchange under ringdown conditions, when all external excitations are turned off and the oscillatory motion is left to decay by dissipation. The two regimes are induced by different sets of initial conditions, and correspond to extremal values of the total net energy transferred during ringdown. Although the problem is in principle fully solvable, its algebraic involvedness requires in practice to resort to approximated expressions for oscillation frequencies and decay rates. We explicitly provide such approximations in the limit of high quality factors and weak coupling. This limit is relevant to current experiments on micro- and nanomechanical oscillators, whose physical behavior is usually explained by extensive allusion to energy exchange. Our results should help to discern between observations that are genuinely due to nonlinear effects, and those that can be explained in terms of linear mechanisms only.

1. Introduction

The dynamics of energy exchange between different degrees of freedom in a mechanical system is a key ingredient of our physical understanding on how the system works, but it is also essential to the design and operation of all kinds of highly relevant technological devices. Controlled processes of energy extraction, harvesting, conversion, and delivery –whose importance escalates in a world where overexploited power sources call for increasingly sophisticated alternatives–are based on the transfer of energy from a natural supply, through some machinery that makes it usable and, ultimately, back to the environment [1, 2]. Careful engineering of energy dissipation is also critical to many applications. Rapid switching between different dynamical regimes, for instance, requires fast damping mechanisms [3, 4]. On the other hand, devices such as pacemakers and certain kinds of sensors base their functioning on the maintenance of oscillatory motion for long periods at low power consumption, which demands small dissipation rates [5–7]. In the laboratory, observation of energy dissipation in a mechanical system is a standard tool to disclose the ingredients that shape its behavior, in particular, the occurrence of nonlinearity [8–11].

In the last two decades, much emphasis has been put on the study of nonlinear effects in the energy exchange of mechanical systems, including how to exploit those effects to get specific dynamical regimes during dissipation [3]. Very recent ringdown experiments on micro- and nanomechanical oscillators –where an initial external forcing is suddenly turned off, and oscillations are left to die out by damping–have disclosed the occurrence of one or more transitions between time intervals where oscillation amplitudes decay at different rates [12, 13]. This kind of behavior has been ascribed to nonlinearity both in the intrinsic dynamics of the

oscillators and in the coupling between their various oscillation modes. In fact, micro- and nanomechanical oscillators are well-known instances of nonlinear systems [14]. Models including anharmonic restoring forces, as well as nonlinear coupling, have successfully reproduced their many dynamical regimes [12, 13, 15, 16].

What it is not so clear, however, is to which extent one must always invoke nonlinearity to explain a given empirical observation on a nonlinear mechanical system. Indeed, the fact that the system involves anharmonic forces does not automatically mean that nonlinearity reveals itself in all the dynamical features, or that such features could never be present in a purely linear system. To clarify this point in connection with the experiments on micro- and nanomechanical oscillators mentioned above, in this paper we revisit the classical problem of two coupled *linear* damped mechanical oscillators [17], with emphasis on their mutual exchange of energy. Coupled-oscillator models, in fact, yield a standard description for modal interaction in vibrating solid bodies, ranging from the beams of building structures to the components of microscopic machines [18, 19]. Our main aim is to characterize as completely as possible the different regimes associated with energy exchange between the two oscillators, thus providing a reference set of results with which empirical observations can be contrasted.

After presenting the equations of motion for our system, stationary and ringdown solutions are numerically and analytically studied in sections 2 and 3, with emphasis in the dynamics of energy exchange. Section 4 is devoted to a summary of the results, and to a discussion in connection with experimental observations.

2. Equations of motion and stationary oscillations

We consider two harmonic oscillators with coordinates $x_1(t)$ and $x_2(t)$ and masses m_1 and m_2, coupled through a bilinear interaction potential $V_{\rm int} = -Jx_1x_2$. An external harmonic force of amplitude F and frequency Ω is applied to oscillator 1. For the rescaled coordinates $u_1 \equiv x_1$ and $u_2 \equiv \sqrt{m_2/m_1}\,x_2$, the equations of motion, normalized by the respective masses, are

$$\begin{aligned} \ddot{u}_1 + \gamma_1\dot{u}_1 + \omega_1^2 u_1 &= ju_2 + f\cos\Omega t, \\ \ddot{u}_2 + \gamma_2\dot{u}_2 + \omega_2^2 u_2 &= ju_1, \end{aligned} \tag{1}$$

with $\gamma_{1,2} > 0$ the damping coefficients per mass unit, $\omega_{1,2}^2$ the natural frequencies, $j = J/\sqrt{m_1m_2}$, and $f = F/m_1$. The net instantaneous power transferred from oscillator 1 to oscillator 2 due to their interaction is given by the difference between the work per time unit performed by the respective coupling forces:

$$W_{1\to 2} = J(x_1\dot{x}_2 - \dot{x}_1x_2) = jm_1(u_1\dot{u}_2 - \dot{u}_1u_2). \tag{2}$$

Our main results in the following sections concern this quantity, both during forced stationary oscillations ($f \neq 0$) and during ringdown ($f = 0$).

Naturally, being equivalent to a set of four linear first-order differential equations, the equations of motion (1) can formally be given a full solution, in terms of eigenvalues and eigenvectors of the related fourth-order algebraic problem [20]. This result, in turn, can be replaced into (2) to explicitly compute $W_{1\to 2}$. In practice, however, the general solution can hardly be cast in a workable form, mainly due to the involved expression of the eigenvalues, which are the roots of a fourth-degree polynomial. Therefore, our strategy is to work within approximations that allow for more compact expressions and that, at the same time, are relevant to the experimental conditions with micro- and nanomechanical oscillators. Similarly, we do not switch to the standard eigenvector representation of a linear problem such as (1), but preserve the description in term of the original coordinates $u_{1,2}$ and their velocities, which are expected to be directly observable quantities in the experiments.

Under the action of the external harmonic forcing $f\cos\Omega t$, and after a transient whose length is controlled by the damping coefficients $\gamma_{1,2}$ (see section 3), the system asymptotically attains a stationary state where the two oscillators perform synchronized motion with the same frequency as the external force. Namely, $u_{1,2}(t) = A_{1,2}\cos(\Omega t + \phi_{1,2}) \equiv {\rm Re}[a_{1,2}\exp(i\Omega t)]$, with $a_{1,2} = A_{1,2}\exp(i\phi_{1,2})$. Without generality loss, we assume $A_{1,2} \geqslant 0$ and $f, \Omega > 0$. This form of $u_{1,2}(t)$ is a solution to (1) if

$$a_1 = \frac{L_2 f}{L_1L_2 - j^2}, \qquad a_2 = \frac{jf}{L_1L_2 - j^2}, \tag{3}$$

with $L_{1,2} = \omega_{1,2}^2 - \Omega^2 + i\gamma_{1,2}\Omega$.

It is customary to characterize the resonant response of an oscillating system to harmonic external forcing of frequency Ω by specifying the oscillation amplitudes and phases as functions of Ω [21]. A more comprehensive description –absorbing all the parameters into non-dimensional rescaled quantities–is obtained in the present case in terms of the rescaled detunings

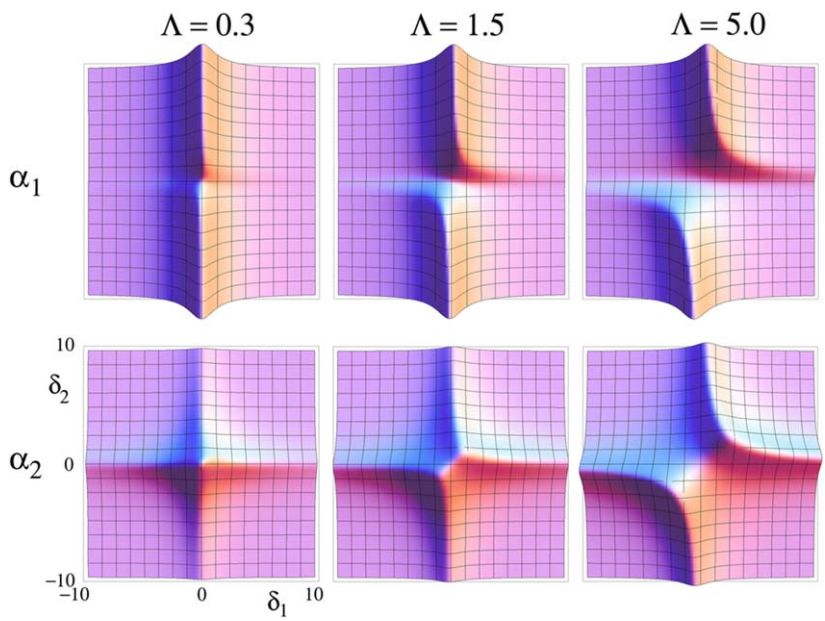

Figure 1. The rescaled oscillation amplitudes α_1 (upper panels) and α_2 (lower panels), given by (5), as functions of the detunings $\delta_{1,2}$ in (4), for three values of the coupling parameter Λ. The scales for all the panels are the same as indicated in the lower-left plot.

$$\delta_{1,2} = \frac{\omega_{1,2}^2 - \Omega^2}{\gamma_{1,2}\Omega}. \tag{4}$$

The rescaled oscillation amplitudes read

$$\alpha_1 \equiv \frac{\gamma_1\Omega}{f}A_1 = \frac{\sqrt{\delta_2^2+1}}{\Delta}, \quad \alpha_2 \equiv \frac{\gamma_1\gamma_2\Omega^2}{|j|f}A_2 = \frac{1}{\Delta}, \tag{5}$$

with

$$\Delta = \sqrt{(\Lambda + 1 - \delta_1\delta_2)^2 + (\delta_1+\delta_2)^2}, \quad \Lambda = \frac{j^2}{\gamma_1\gamma_2\Omega^2}. \tag{6}$$

Note that, except for the proportionality $\alpha_2 \propto |j|^{-1}$, the positive non-dimensional parameter Λ captures all the information about the coupling strength between the oscillators. These results, moreover, are independent of the sign of j.

In figure 1, we show plots of the rescaled amplitudes $\alpha_{1,2}$ as functions of the detunings $\delta_{1,2}$ for three values of the coupling parameter Λ. For small Λ, as expected for ordinary resonance under the action of harmonic forcing, the amplitude of oscillator 1 is maximal when its own detuning δ_1 is close to zero. A small downward indentation in α_1 appears however around $\delta_2 = 0$, where oscillator 2 is best tuned to resonantly receive the energy transferred from the external force through oscillator 1. Correspondingly, α_2 displays resonance ridges around the axes $\delta_1 = 0$ and $\delta_2 = 0$, and attains its maximum when the two oscillators are perfectly tuned to the force ($\delta_1 = \delta_2 = 0$). As coupling becomes stronger and Λ increases, the indentation in α_1 grows deeper, indicating that energy transfer to oscillator 2 is more efficient. At the same time, both for α_1 and α_2, the points of maximal amplitude shift from the axes toward larger detunings. For $\Lambda = 1$, specifically, the maximum of α_2 becomes a saddle point, and two lateral maxima appear in the quadrants where $\delta_{1,2}$ have equal signs. The shift of resonance ridges to nonzero detuning as Λ grows is associated with a change in the oscillation frequencies, induced by linear coupling (see section 3).

Equations (5) and (6) readily show that, as illustrated by figure 1, the width of the resonance ridges is always of order unity in the rescaled detunings $\delta_{1,2}$, irrespectively of the value of the coupling parameter Λ. In contrast, as advanced in the preceding paragraph, the position of the resonance ridges is strongly dependent on Λ, with a qualitative change of behavior at $\Lambda \approx 1$. For $\Lambda \ll 1$, (5) reduces to

$$\alpha_1 \approx \frac{1}{\sqrt{\delta_1^2+1}}, \qquad \alpha_2 \approx \frac{1}{\sqrt{(\delta_1^2+1)(\delta_2^2+1)}}, \tag{7}$$

which clearly represent the resonance ridges along the axes $\delta_1 = 0$ and $\delta_2 = 0$, with a cusp in α_2 for $\delta_1 = \delta_2 = 0$. For $\Lambda \gg 1$, on the other hand, the ridges occur along the hyperbola $\delta_2 = \Lambda/\delta_1$. On this curve, the amplitudes are

$$\alpha_1 \approx \frac{\Lambda}{\delta_1^2 + \Lambda}, \qquad \alpha_2 \approx \frac{|\delta_1|}{\delta_1^2 + \Lambda}. \tag{8}$$

For the stationary motion considered here, the oscillation phases $\phi_{1,2}$ are defined up to an arbitrary additive constant. The only relevant quantity associated to them is therefore the phase difference $\phi_1 - \phi_2$, given through

$$\cos(\phi_1 - \phi_2) = \frac{\delta_2\ \mathrm{sgn}(j)}{\sqrt{\delta_2^2 + 1}}, \qquad \sin(\phi_1 - \phi_2) = \frac{\mathrm{sgn}(j)}{\sqrt{\delta_2^2 + 1}}. \tag{9}$$

Note that whether one of the phases is ahead or behind the other depends on the sign of the interaction constant, $\mathrm{sgn}(j)$.

The phase difference appears in the expression for the net power transfer $W_{1\to 2}$ of (2):

$$W_{1\to 2} = jm_1 A_1 A_2 \Omega \sin(\phi_1 - \phi_2) = |j| m_1 \frac{A_1 A_2 \Omega}{\sqrt{\delta_2^2 + 1}}. \tag{10}$$

Remarkably, in spite of the oscillatory dynamics of the system, $W_{1\to 2}$ is constant in time. Moreover, it is always positive, indicating that a sustained energy flux occurs from oscillator 1 –where energy is injected by the external force–to oscillator 2. Using the rescaling for the amplitudes introduced in (5), the corresponding non-dimensional expression for the power transfer turns out to be equal to α_2^2. Therefore, the dependence of the power transfer on the detunings $\delta_{1,2}$ is qualitatively well illustrated by the lower row of figure 1.

3. Ringdown dynamics

3.1. Approximations for the eigenvalues

In the absence of external forcing, $f = 0$ in (1), and for moderate values of the damping coefficients $\gamma_{1,2}$, the motion of our system consists of damped oscillations, with decaying, asymptotically vanishing amplitudes. The solutions $u_{1,2}(t)$ can be explicitly written down as linear combinations of the exponentials $\exp(\lambda_{a,b}^{\pm} t)$, where the two pairs of complex-conjugate numbers $\lambda_{a,b}^{\pm} = -\mu_{a,b} \pm i\Omega_{a,b}$ are the eigenvalues of the Jacobian

$$\mathcal{J} = \begin{pmatrix} 0 & 0 & 1 & 0 \\ 0 & 0 & 0 & 1 \\ -\omega_1^2 & j & -\gamma_1 & 0 \\ j & -\omega_2^2 & 0 & -\gamma_2 \end{pmatrix}. \tag{11}$$

Their real parts are always negative ($\mu_{a,b} > 0$) and control the exponential decay of the amplitudes. Their imaginary parts, in turn, are given by the 'non-normal' oscillation frequencies $\Omega_{a,b}$ (which do not coincide with the normal-mode frequencies of the undamped system [17]). Without generality loss, we choose $\Omega_{a,b} > 0$. The solutions $\exp(\lambda_{a,b}^{\pm} t)$ also describe, in the case with external forcing considered in the preceding section, the transient motion toward stationary oscillations.

In principle, being the roots of a fourth-degree polynomial, the eigenvalues $\lambda_{a,b}^{\pm}$ can be written out explicitly. Practical approximate expressions, however, can only be obtained in suitable limits. In the following, we focus on the limit $\gamma_{1,2} \ll \omega_{1,2}$. Indeed, in systems where energy exchange between oscillating modes has a significant dynamical role, it is expected that the times associated with energy dissipation (of order $\gamma_{1,2}^{-1}$) are much longer than the typical oscillation periods (of order $\omega_{1,2}^{-1}$). This limit is relevant to applications to micro- and nanomechanical oscillators, on which we focus in this paper. The quality factor of such devices –given by the ratio between the frequency and the damping coefficient, $Q = \omega/\gamma$–can in fact reach values from 10^4 to 10^8 [12, 15, 22]. In experiments with macroscopic oscillators –ranging from pendulums, to vibrating strings, to cantilevers–typical quality factors are $Q \sim 10^2$ to 10^3 [23, 24], so that the limit still holds.

In externally forced linear oscillators, the quality factor is an inverse measure of the width of the resonance peak relative to the frequency of the external force: the larger the value of Q, the narrower the resonance frequency band. In connection with this feature, the assumption of high quality factors in our two-oscillator system brings about a further simplification. In fact, sizable dynamical effects of the interaction between the two oscillators are only expected when their natural frequencies are not too far from each other, so that their mutual resonance peaks overlap with each other. This condition requires $|\omega_1 - \omega_2| \lesssim \gamma_{1,2}$. Combined with the assumption of high Q, $\gamma_{1,2} \ll \omega_{1,2}$, it makes it possible to restrict the analysis to the case of identical natural frequencies, $\omega_1 = \omega_2 \equiv \omega$, as we do hereafter.

From the viewpoint of the mathematical procedure, it turns out that the limit of weak damping, $\gamma_{1,2} \to 0$, cannot be taken irrespectively of the value of the rescaled coupling constant j. In fact, as for the stationary oscillations analyzed in section 2, the behavior of the system depends on how the interaction forces compare with damping forces –cf the non-dimensional parameter Λ in (6). Therefore, it is necessary to consider as two separate cases the limits $\gamma_{1,2} \to 0$ and $j \to 0$, even when the condition of high Q, $\gamma_{1,2} \ll \omega$, must always hold. In

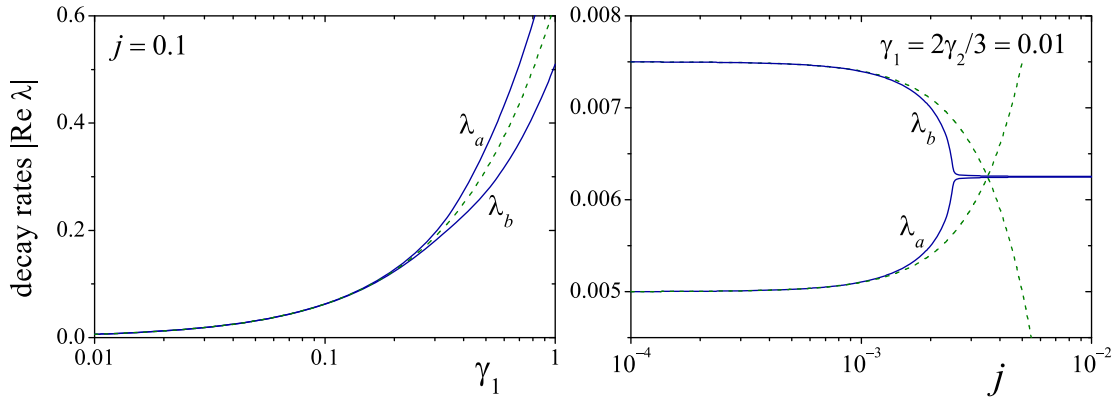

Figure 2. Left: decay rates (given by the absolute value of the real part of Jacobian eigenvalues) for $\omega_1 = \omega_2 \equiv \omega = 1, j = 0.1$, as functions of γ_1, with $\gamma_2 = 3\gamma_1/2$. Full lines: exact vales; dashed line: weak-damping approximation, given by (13). Right: decay rates for $\omega = 1$ and $\gamma_1 = 2\gamma_2/3 = 0.01$, as functions of j. Full lines: exact values; dashed lines: weak-coupling approximation, given by (15).

both cases, our approach is the same: we find the exact eigenvalues of the Jacobian for either $\gamma_{1,2} = 0$ or $j = 0$ as the roots of the corresponding fourth-order polynomial and, then, we obtain approximate solutions to the first significant order, as perturbations of those exact roots.

3.1.1. Weak damping

For $\gamma_{1,2} = 0$, the eigenvalues of $\mathcal{J}$ in (11) are

$$\lambda^{\pm}_{a,b}(\gamma_{1,2} = 0) = \pm i\sqrt{\omega^2 \pm j}. \tag{12}$$

As expected, these imaginary roots describe undamped, purely oscillating solutions. Note, however, that this requires that coupling is not too large, i.e. $j < \omega^2$.

The first significant correction to this result adds a real part to the eigenvalues, without changing their imaginary parts, namely:

$$\lambda^{\pm}_{a,b} \approx -\frac{\gamma_1 + \gamma_2}{4} \pm i\sqrt{\omega^2 \pm j}. \tag{13}$$

This correction is the same for the two pairs of complex-conjugate eigenvalues and does not depend on the coupling constant j. To the next order, the correction is proportional to $\gamma^2_{1,2}/\omega \ll \gamma_{1,2}$ and only affects the imaginary parts of $\lambda^{\pm}_{a,b}$. The leftmost panel of figure 2 compares the approximated decay rates given by (13) (dashed line) with the exact values (full lines) for selected parameters.

For weak damping, thus, the oscillation amplitude decays at a uniform rate, independent of the coupling strength, within a typical time scale of order $(\gamma_1 + \gamma_2)^{-1}$. Oscillations, in turn, are generally given by the combination of two harmonic motions of different frequencies.

3.1.2. Weak coupling

In contrast with the previous case, for $j = 0$ the eigenvalues of $\mathcal{J}$ have both real and imaginary parts:

$$\lambda^{\pm}_{a,b}(j = 0) = -\frac{1}{2}\gamma_{1,2} \pm i\sqrt{\omega^2 - \frac{1}{4}\gamma^2_{1,2}} \approx -\frac{1}{2}\gamma_{1,2} \pm i\omega. \tag{14}$$

Not unexpectedly, each complex-conjugate pair involves the damping coefficient of only one of the two oscillators.

The first significant correction in the limit of weak coupling affects both the decay rates and the frequencies:

$$\lambda^{\pm}_{a,b} \approx -\frac{\gamma_{1,2}}{2}\left(1 + \frac{j^2}{\gamma_{1,2}g_{1,2}\omega^2}\right) \pm i\omega\left(1 + \frac{j^2\gamma_1\gamma_2}{4g^2_{1,2}\omega^4}\right), \tag{15}$$

with $g_1 = -g_2 = \gamma_2 - \gamma_1$. Note that the new terms are quadratic in the coupling constant. Moreover, the relative correction to the imaginary part is of order $\gamma^2_{1,2}/\omega^2 \ll 1$ as compared to that of the real part. A comparison of the approximated and exact decay rates for selected values of the parameters is shown in the rightmost panel of figure 2.

3.2. Explicit ringdown solution

Once the eigenvalues $\lambda_{a,b}^{\pm} = -\mu_{a,b} \pm i\Omega_{a,b}$ have been obtained –either exactly, or within any suitable approximation–we can explicitly write down the general solution to the first of equations (1) as

$$u_1(t) = A_a e^{-\mu_a t}\cos(\Omega_a t + \phi_a) + \{b\}, \tag{16}$$

where $\{b\}$ stands for a term with the same form as the preceding one, except that all subindices are b instead of a. For the second of equations (1), the solution is

$$u_2(t) = j^{-1}A_a e^{-\mu_a t}[C_a\cos(\Omega_a t + \phi_a) + S_a\sin(\Omega_a t + \phi_a)] + \{b\}, \tag{17}$$

with

$$C_{a,b} = \omega_1^2 - \Omega_{a,b}^2 + \mu_{a,b}(\mu_{a,b} - \gamma_1), \qquad S_{a,b} = \Omega_{a,b}(2\mu_{a,b} - \gamma_1). \tag{18}$$

The amplitudes $A_{a,b}$ and the phases $\phi_{a,b}$ are arbitrary constants, whose values become determined when a suitable set of initial conditions is specified. Fixing the coordinates $u_{1,2}(0)$ and the velocities $\dot{u}_{1,2}(0)$ at time $t = 0$, amplitudes and phases can be obtained from the following set of equations:

$$\begin{aligned} u_1(0) &= A_a\cos\phi_a + \{b\},\\ ju_2(0) &= A_a(C_a\cos\phi_a + S_a\sin\phi_a) + \{b\},\\ -\dot{u}_1(0) &= A_a(\mu_a\cos\phi_a + \Omega_a\sin\phi_a) + \{b\},\\ -j\dot{u}_2(0) &= A_a[\mu_a(C_a\cos\phi_a + S_a\sin\phi_a)\\ &\quad + \Omega_a(C_a\sin\phi_a - S_a\cos\phi_a)] + \{b\}. \end{aligned} \tag{19}$$

This system is linear in the products $A_{a,b}\cos\phi_{a,b}$ and $A_{a,b}\sin\phi_{a,b}$, which can therefore be immediately found to later compute $A_{a,b}$ and $\phi_{a,b}$.

Equations (16) to (19) complete the solution to the present problem. From now on, we focus the attention on the exchange of energy between the two oscillators. The net instantaneous power transfer from oscillator 1 to oscillator 2, $W_{1\to 2}$, is given by (2). This quantity has an explicit simplified form in the relevant limit of weak damping and coupling, $\gamma_{1,2}$, $j^{1/2} \ll \omega_{1,2}$, already discussed in section 3.1. In this limit, as shown by (13) and (15), the frequencies $\Omega_{a,b}$ differ from each other by a small quantity. Assuming, without generality loss, that $\Omega_a > \Omega_b$, they can be written as

$$\Omega_{a,b} = \Omega_0 \pm \frac{\nu}{2}, \tag{20}$$

where $\Omega_0 = (\Omega_a + \Omega_b)/2$ and $\nu = \Omega_a - \Omega_b \ll \Omega_0$, with $\nu > 0$. Because of a partial compensation of the oscillations in the power transferred by the interaction forces, $Jx_1\dot{x}_2$ and $J\dot{x}_1x_2$, the dominant oscillating contributions to $W_{1\to 2}$ have frequency ν:

$$\begin{aligned} (m_1\Omega_0)^{-1}W_{1\to 2} \approx\ & S_aA_a^2e^{-2\mu_a t} + S_bA_b^2e^{-2\mu_b t} + A_aA_be^{-(\mu_a+\mu_b)t}\\ & \times[(S_a + S_b)\cos(\nu t + \Phi) - (C_a - C_b)\sin(\nu t + \Phi)], \end{aligned} \tag{21}$$

with $\Phi = \phi_a - \phi_b$. The long-time behavior of $W_{1\to 2}$ is controlled by the term in (21) with the slowest exponential decay. Assuming, without generality loss, that $\mu_a < \mu_b$, the asymptotic power transfer is

$$(m_1\Omega_0)^{-1}W_{1\to 2}(t\to\infty) \approx S_aA_a^2e^{-2\mu_a t}, \tag{22}$$

whose sign is determined by that of S_a. Using (13) and (15), it can readily be shown that, within the approximations considered in section 3.1, the sign of S_a is always the same as that of the difference $g_1 = \gamma_2 - \gamma_1$. For long times, therefore, the net flux of energy always occurs from the oscillator with the smaller damping coefficient toward that with the larger damping coefficient. Power is thus transferred by coupling to the oscillator with higher capacity to dissipate energy.

The total energy transferred from oscillator 1 to oscillator 2 along the whole ringdown process, $E_{1\to 2}^{\mathrm{tot}} = \int_0^\infty W_{1\to 2}dt$, is given by

$$\begin{aligned} (m_1\Omega_0)^{-1}E_{1\to 2}^{\mathrm{tot}} \approx\ & \frac{S_aA_a^2}{2\mu_a} + \frac{S_bA_b^2}{2\mu_b}\\ & + A_aA_b\frac{(S_a + S_b)\sin(\Phi_0 - \Phi) - (C_a - C_b)\cos(\Phi_0 - \Phi)}{\sqrt{(\mu_a + \mu_b)^2 + \nu^2}}, \end{aligned} \tag{23}$$

with $\sin\Phi_0 = (\mu_a + \mu_b)\big/\sqrt{(\mu_a + \mu_b)^2 + \nu^2}$, $\cos\Phi_0 = \nu\big/\sqrt{(\mu_a + \mu_b)^2 + \nu^2}$. In the following, $E_{1\to 2}^{\mathrm{tot}}$ is used to discern between different ways in which energy is exchanged during the ringdown dynamics.

3.3. Different regimes of energy exchange

Different dynamical regimes of energy exchange during ringdown can be characterized by the extremal (maximal or minimal) values of $E^{\rm tot}_{1\to 2}$. For a given set of parameters, such regimes would ultimately be determined by the initial conditions, as explained in the following.

Expansion of (23) straightforwardly shows that, within the approximations considered in section 3.2, the total energy transferred during ringdown is a homogeneous quadratic function of the products $A_{a,b}\cos\phi_{a,b}$ and $A_{a,b}\sin\phi_{a,b}$. Namely, $E^{\rm tot}_{1\to 2}$ is a linear combination of terms given by the multiplication of two of those products. Via (19), in turn, we can express the products as linear combinations of the initial conditions. Consequently, $E^{\rm tot}_{1\to 2}$ is also a quadratic function of the initial conditions. In other words, introducing the vector of initial conditions $\mathbf{U}=(u_1(0),\,u_2(0),\,\dot u_1(0),\,\dot u_2(0))$, there exists a matrix $\mathcal{Q}$ such that $E^{\rm tot}_{1\to 2}=\mathbf{U}^\dagger\mathcal{Q}\mathbf{U}$. The elements of $\mathcal{Q}$ depend on the system parameters only. Extremization of $E^{\rm tot}_{1\to 2}$ with respect to the initial conditions thus amounts to solving the equation $\nabla_{\mathbf{U}}(\mathbf{U}^\dagger\mathcal{Q}\mathbf{U})=0$. This calculation, however, cannot be done on the unrestricted set of all possible initial conditions: otherwise, we would obtain trivial solutions with $|\mathbf{U}|\to\infty$ and $|\mathbf{U}|\to 0$, for which $E^{\rm tot}_{1\to 2}$ reaches arbitrarily large and small values, respectively.

A reasonable constraint to perform the extremization is to require that all the initial conditions correspond to the same initial value of the total energy,

$$\begin{aligned}E_0&=\frac{m_1}{2}\dot x_1(0)^2+\frac{m_2}{2}\dot x_2(0)^2+\frac{m_1\omega_1^2}{2}x_1(0)^2+\frac{m_2\omega_2^2}{2}x_2(0)^2-Jx_1(0)x_2(0)\\&=\frac{m_1}{2}[\dot u_1(0)^2+\dot u_2(0)^2+\omega_1^2u_1(0)^2+\omega_2^2u_2(0)^2]-jm_1u_1(0)u_2(0).\end{aligned}\tag{24}$$

We note that this also is a homogeneous quadratic function of $\mathbf{U}$. Namely, there is a matrix $\mathcal{E}$ such that $E_0=\mathbf{U}^\dagger\mathcal{E}\mathbf{U}$. As in the case of $\mathcal{Q}$, the elements of $\mathcal{E}$ depend on the system parameters only. The extremization of $E^{\rm tot}_{1\to 2}$ on the manifold where the initial energy is a prescribed value E_0 results from the equation $\nabla_{\mathbf{U}}[\mathbf{U}^\dagger\mathcal{Q}\mathbf{U}+\rho(E_0-\mathbf{U}^\dagger\mathcal{E}\mathbf{U})]=0$, where ρ is a Lagrange multiplier. This problem turns out to be equivalent to solving the eigenvalue equation

$$(\mathcal{E}^{-1}\mathcal{Q})\mathbf{U}=\rho\mathbf{U}.\tag{25}$$

In other words, the eigenvectors resulting from (25) give the initial conditions for which $E^{\rm tot}_{1\to 2}$ adopts its extremal values, with the constraint that the initial energy E_0 is fixed.

Note that E_0 does not appear in (25). Therefore, the corresponding eigenvectors and eigenvalues can first be found as functions of the system parameters only. Then, the eigenvectors can be rescaled by a suitable factor, in such a way that the identity $E_0=\mathbf{U}^\dagger\mathcal{E}\mathbf{U}$ is fulfilled for the desired value of the initial energy. The respective eigenvalues –which are not affected by the eigenvector rescaling–give the ratio between the total energy transferred during ringdown and the initial energy: $\rho=E^{\rm tot}_{1\to 2}/E_0$.

While the matrix that defines the initial total energy can be immediately written down, as

$$\mathcal{E}=\frac{m_1}{2}\begin{pmatrix}\omega_1^2&-j&0&0\\-j&\omega_2^2&0&0\\0&0&1&0\\0&0&0&1\end{pmatrix},\tag{26}$$

generally, the matrix $\mathcal{Q}$ cannot be given a compact expression. However, under the conditions of high quality factors and weak coupling considered in section 3.1.2, it approaches the simple form

$$\mathcal{Q}^0=\frac{m_1 j}{\gamma_1+\gamma_2}\begin{pmatrix}0&0&0&1\\0&0&-1&0\\0&-1&0&0\\1&0&0&0\end{pmatrix}\tag{27}$$

when $j\to 0$. In the same limit, the matrix $\mathcal{E}$ becomes diagonal,

$$\mathcal{E}^0=\frac{m_1}{2}\begin{pmatrix}\omega^2&0&0&0\\0&\omega^2&0&0\\0&0&1&0\\0&0&0&1\end{pmatrix},\tag{28}$$

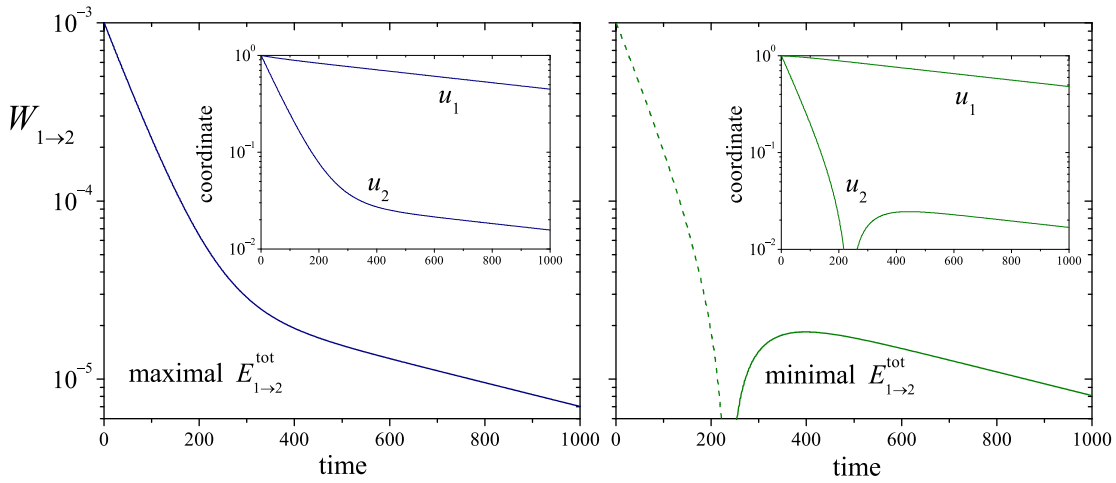

Figure 3. Main plots: power transfer $W_{1\to2}$ as a function of time, obtained from numerical resolution of (1) for $\omega_1 = 1, \omega_2 = 1.001$, $\gamma_1 = 0.001\,5, \gamma_2 = 0.03, j = 0.001$, with unitary initial energy, $E_0 = 1$, for initial conditions $\mathbf{U}_1$ and $\mathbf{U}_4$, respectively corresponding to maximal (left) and minimal (right) total energy transfer $E^{tot}_{1\to2}$. Dashed lines indicate negative values of $W_{1\to2}$. Insets: Positive envelopes of the coordinates u_1 and u_2 as functions of time, for the same cases as in the respective main plots.

and the eigenvalue problem (25) can be readily solved. The resulting eigenvectors and eigenvalues are

$$\begin{aligned}
\mathbf{U}_1^0 &= v_0(1,\ 1,\ -\omega,\ \omega), \qquad \rho_1^0 = r_0,\\
\mathbf{U}_2^0 &= v_0(-1,\ 1,\ -\omega,\ -\omega), \quad \rho_2^0 = r_0,\\
\mathbf{U}_3^0 &= v_0(1,\ 1,\ \omega,\ -\omega), \qquad \rho_3^0 = -r_0,\\
\mathbf{U}_4^0 &= v_0(-1,\ 1,\ \omega,\ \omega), \qquad \rho_4^0 = -r_0,
\end{aligned} \tag{29}$$

with $v_0 = \sqrt{E_0/2\omega^2 m_1}$ and $r_0 = 2j/(\gamma_1 + \gamma_2)\omega$. We see that $\mathbf{U}_1^0$ and $\mathbf{U}_2^0$ on one side, and $\mathbf{U}_3^0$ and $\mathbf{U}_4^0$ on the other, form pairs of degenerate eigenvectors. Moreover, if $j > 0$, the initial conditions given by $\mathbf{U}_1^0$ and $\mathbf{U}_2^0$ correspond to a positive extremum of the total energy transfer during ringdown: $E^{tot}_{1\to2} = 2jE_0/(\gamma_1 + \gamma_2)\omega$. For $\mathbf{U}_3^0$ and $\mathbf{U}_4^0$, the extremum of $E^{tot}_{1\to2}$ has the same modulus and opposite sign. If $j < 0$, these relations are interchanged. In the following, we use this limit case as a reference situation for the numerical characterization of the dynamics of energy exchange between the two oscillators.

3.3.1. Numerical results

We have explored the problem of extremization of $E^{tot}_{1\to2}$ numerically, for selected values of the parameters. In all cases, without generality loss, we have chosen $\gamma_2 > \gamma_1$. According to our discussion around (22), such choice implies that, for sufficiently long times, the energy always flows from oscillator 1 to oscillator 2, i.e. $W_{1\to2}(t \to \infty) > 0$.

Within the approximation of large quality factor and weak coupling, but for finite values of j, numerical solution of the eigenvalue problem (25) shows that the degeneracy of the eigenvectors in (29) breaks down. Specifically, for $j > 0$, the eigenvector $\mathbf{U}_1$ ($\approx\mathbf{U}_1^0$) corresponds to a maximum of $E^{tot}_{1\to2}$, while $\mathbf{U}_2$ ($\approx\mathbf{U}_2^0$) is a saddle point. Namely, the respective eigenvalues verify $\rho_1 \gtrsim \rho_2$. As for the other two eigenvectors, $\mathbf{U}_4$ ($\approx\mathbf{U}_4^0$) corresponds to a minimum of the total energy transfer, while $\mathbf{U}_3$ ($\approx\mathbf{U}_3^0$) is another saddle point, with $\rho_3 \gtrsim \rho_4$. For $j < 0$ the relations are inverted, with $\mathbf{U}_1$ and $\mathbf{U}_4$ respectively corresponding to the minimum and the maximum of $E^{tot}_{1\to2}$.

To study the dynamics of energy exchange during ringdown, we have performed numerical integration of the ringdown version of (1) –namely, with $f = 0$–using a standard fourth-order Runge-Kutta scheme. In order to obtain more generic results, we relaxed the approximation $\omega_1 = \omega_2$ used in our analytical derivations, although the condition $|\omega_1 - \omega_2| \lesssim \gamma_{1,2}$, relevant to the limit of high quality factor (see section 3.1), was maintained. We have explored a variety of parameters compatible with a high quality factor and weak coupling, verifying that initial conditions corresponding to the extremal values of $E^{tot}_{1\to2}$ indeed characterize different regimes of energy exchange.

As an illustration, the main plots in figure 3 show the net instantaneous power transferred from oscillator 1 to oscillator 2, $W_{1\to2}$, as a function of time, for $\omega_1 = 1, \omega_2 = 1.001, \gamma_1 = 0.001\,5, \gamma_2 = 0.03$, and $j = 0.001$. We have used dashed lines to indicate negative values of $W_{1\to2}$. In all cases, the initial energy, given by (24), has been fixed at $E_0 = 1$. For these parameters, using $m_1 = 1$, the eigenvectors and eigenvalues are as follows:

$$\begin{aligned}
\mathbf{U}_1 &= (0.67,\ 0.71,\ -0.74,\ 0.71), & \rho_1 &= 0.059\,6,\\
\mathbf{U}_2 &= (-0.74,\ 0.70,\ -0.67,\ -0.71), & \rho_2 &= 0.058\,8,\\
\mathbf{U}_3 &= (0.74,\ 0.70,\ 0.67,\ -0.71), & \rho_3 &= -0.067\,6,\\
\mathbf{U}_4 &= (-0.67,\ 0.71,\ 0.74,\ 0.71), & \rho_4 &= -0.068\,6,
\end{aligned} \tag{30}$$

cf (29). In the leftmost panel, we used the initial condition $\mathbf{U}_1$, for which $E^{\rm tot}_{1\to 2}$ attains its maximum. We see that $W_{1\to 2}(t)$ is always positive, with a monotonous decay as time elapses. Clearly, the evolution of $W_{1\to 2}(t)$ in this regime is divided into two stages. In the first one, the dynamics is dominated by the largest decay rate, $2\mu_b \approx \gamma_2$. In the second, when the component decaying at rate $2\mu_b$ has died out, dominance is overtaken by the smallest decay rate, $2\mu_a \approx \gamma_1$, which controls the final approach to rest. This separation results into two well defined slopes in different zones of the logarithmic plot.

The rightmost panel of figure 3 shows the power transferred as a function of time for the same parameters, but with the initial condition $\mathbf{U}_4$, which corresponds to the minimum of $E^{\rm tot}_{1\to 2}$. For this initial condition, $W_{1\to 2}(t)$ is initially negative, so that energy flows from oscillator 2 to oscillator 1. Eventually, as expected from (22), this sign is reversed and the final decay of $W_{1\to 2}(t)$ occurs from the positive side. It is the balance between stages with opposite signs for the instantaneous energy exchange that explains the minimal value of the total energy transferred between the oscillators. As a matter of fact, as it results from the eigenvalues reported in (30), in this case $E^{\rm tot}_{1\to 2} < 0$.

The insets in the two panels of figure 3 show the oscillation amplitudes of the two oscillators –as given by the (positive) envelopes of the coordinates u_1 and u_2–as functions of time. We see that the amplitude of oscillator 1 decays at a practically constant rate, $\mu_a \approx \gamma_1/2$, which is controlled by its own damping coefficient. In turn, the amplitude of oscillator 2 'copies' the time behavior of $W_{1\to 2}$, with a clear change in its decay rate for the initial condition given by $\mathbf{U}_1$, and nonmonotonic evolution for $\mathbf{U}_4$. Note that the long-time amplitude decay rates are the same in all cases.

When the initial condition is taken as given by the eigenvector $\mathbf{U}_2$ –which, as mentioned before, correspond to a saddle point of $E^{\rm tot}_{1\to 2}$–the evolution of $W_{1\to 2}(t)$ is practically identical to that obtained from $\mathbf{U}_1$. Comparing (30), it is clear that $\mathbf{U}_1$ and $\mathbf{U}_2$ represent quite different initial conditions, in particular, regarding the relative signs of positions and velocities of the two oscillators. These differences, however, compensate each other when calculating the products that define the net power transfer, given by (2), and the resulting value of $W_{1\to 2}(t)$ is virtually the same. Note that, in spite of the differences between the eigenvalues $\mathbf{U}_1$ and $\mathbf{U}_2$, their eigenvalues ρ_1 and ρ_2 are mutually very similar. This reinforces the notion that the value of $E^{\rm tot}_{1\to 2}$ is a good indicator of the dynamical regime of energy exchange between the two oscillators. A similar situation is met when comparing the evolution from the initial conditions $\mathbf{U}_3$ (saddle point) and $\mathbf{U}_4$ (minimum).

The crossover between the two regimes shown in figure 3 can be characterized by considering initial conditions of the form $\mathbf{U} = z_{\mathbf{U}}[\epsilon\,\mathbf{U}_1 + (1-\epsilon)\,\mathbf{U}_4]$, which linearly interpolates between the initial conditions that lead to maximal and minimal energy exchange. The prefactor $z_{\mathbf{U}}$ is chosen in such a way that $\mathbf{U}$ corresponds to an initial total energy $E_0 = 1$. Figure 4 shows that, for $\epsilon = 0.55$, the evolution of $W_{1\to 2}$ is qualitatively similar to the case $\epsilon = 1$, for which two stages with different decay rates are clearly discerned. For $\epsilon = 0.45$, on the other hand, we find a situation similar to $\epsilon = 0$, with an initial stage of negative $W_{1\to 2}$, followed by the final decay where $W_{1\to 2} > 0$ (cf, respectively, leftmost and rightmost panel of figure 3). The two regimes are mediated by the appearance of an intervening time interval where $W_{1\to 2} < 0$, which hints at an oscillation in the power transfer ($\epsilon = 0.51$). For $\epsilon = 0.5$, the lower end of the interval attains the initial time $t = 0$. Note that, over all this crossover region, the typical absolute values of the power transfer $W_{1\to 2}$ are orders of magnitude lower than for the cases $\epsilon = 0$ and 1, shown in figure 3.

A clear distinction between the two regimes characterized by maximal and minimal total energy transfer is preserved as long as the limits of high quality factor and weak coupling hold. When the coupling constant j grows, however, the incipient oscillations seen in figure 4 for $\epsilon \approx 0.5$ increasingly dominate the time evolution of the power transfer over wide intervals of the parameters. Figure 5 shows $W_{1\to 2}$ as a function of time for the same parameters as in figure 3 but with a much larger coupling constant, $j = 0.1$. As for smaller j, maximal and minimal values of $E^{\rm tot}_{1\to 2}$ are determined by how the time intervals where $W_{1\to 2}$ is positive or negative partially compensate each other. Now, however, those intervals have greatly increased in number, and the qualitative distinction between the dynamical regimes identified for weak coupling blurs out. In this situation, according to (21), the frequency ν of the oscillations in $W_{1\to 2}$ grows because, as j becomes larger, the difference between the frequencies $\Omega_{a,b}$ increases; cf (13) and (15). At the same time, superimposed fast, small-amplitude oscillations of frequency $\Omega_0 = (\Omega_a + \Omega_b)/2$ –disregarded in the approximation of (21)– become clearly visible.

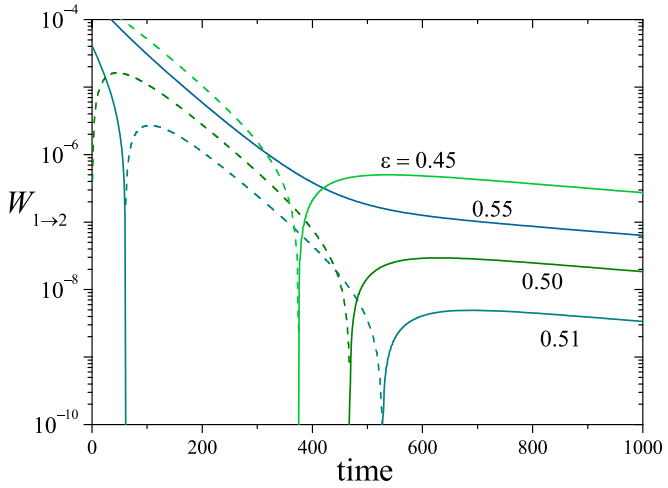

Figure 4. Power transfer $W_{1\to2}$ as a function of time, for the interpolating initial condition $\mathbf{U} = z_{\mathbf{U}}[\epsilon\,\mathbf{U}_1 + (1-\epsilon)\mathbf{U}_4]$ and four values of ϵ. All other parameters are as in figure 3.

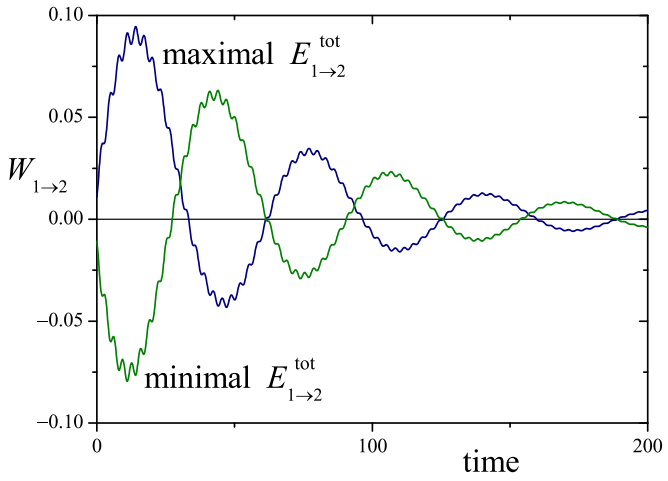

Figure 5. Power transfer $W_{1\to2}$ as a function of time, for the same parameters as in figure 3, except that $j = 0.1$.

4. Summary and discussion

We have here revisited the classical mechanical problem of two harmonic oscillators subjected to damping, and coupled through linear forces, with emphasis on the dynamics of their exchange of energy. Our aim has been to provide a reference set of results with which theoretical and experimental observations on *nonlinear* oscillators can be compared. In fact, in the interpretation of recent experiments on micro- and nanomechanical oscillators –which are driven by anharmonic restoring forces–much emphasis has been put on the role of nonlinear mechanisms in energy exchange and dissipation. However, it is not always clear whether a given dynamical feature must necessarily be ascribed to nonlinearity or could also be observed in a purely linear system, under appropriate conditions.

Although the equations of motion for two coupled linear mechanical oscillators can be fully solved by exploiting their equivalence to a fourth-order algebraic problem, practical analytical expressions are limited to certain approximations. Here, we have focused on the conditions met when working with micro- and nanomechanical oscillators, in particular, on the limit of high quality factors. Under the action of an external harmonic force, stationary oscillations with the same frequency as the force are readily characterized. It turns out that, in spite of the oscillatory nature of the system, the net power transfer between the oscillators is constant in time, and energy always flows from the oscillator subjected to the external force toward the other oscillator.

In ringdown solutions, no external excitation is applied, and motion is left to die out by damping. We have shown that, when the coupling is weak, the long-time net power transfer during ringdown always occurs from the oscillator with the smaller damping coefficient toward the other. Energy thus flows towards the oscillator

where it is dissipated faster. Plausibly, this behavior is related to non-equilibrium thermodynamical principles such as those of extremization of entropy production [25, 26], when extended to non-stationary states.

For shorter times, on the other hand, energy exchange between the oscillators exhibits two well differentiated regimes, depending on the initial conditions. The total energy transferred along the whole ringdown process, toward the oscillator with faster dissipation, can be used to discern between the two regimes. With initial conditions for which this total energy is maximal (leftmost panel of figure 3), the direction of power transfer is the same at all times. In this regime, in turn, the time decay of the power transfer exhibits two separated stages with different decay rates, fast for short times and slow for long times. This separation is associated with the relative dominance of the two decay modes comprised in the solution; cf (16) and (17). In the initial condition, the faster decay mode is dominant but, as time elapses and the corresponding amplitude dies out, the slower mode takes over and controls the final stage. Note that, in this regime, the initial direction of power transfer is the same as in the stationary motion under the action of an external harmonic force. Therefore, in an experiment where ringdown starts from such stationary motion when the external force is suddenly turned off, we expect to observe the two stages with different decay rates as time elapses.

The second regime of energy exchange is characterized by the initial conditions for which the total energy transferred along the whole ringdown process is minimal (rightmost panel of figure 3). In this case, the direction of the initial power transfer is the opposite to that observed for long times. Therefore, a sign change occurs at an intermediate time. A well-defined rate of exponential decay, consequently, can only be observed at the final stage. This long-time decay rate coincides in both regimes. The time behavior of the power transfer for other initial conditions depends on how close they are to either of the extremal cases which characterize the two distinct regimes described above. The crossover between the two regimes occurs for intermediate initial conditions (figure 4), for which the power transfer can change direction more than once. This oscillatory behavior is enhanced as the coupling strength between the oscillators grows. In fact, stronger interactions promote the separation between the oscillation frequencies involved in the motion, which in turn controls the oscillations of the power transfer; cf (13), (15), and (21). Numerical results show that, for sufficiently strong coupling, the power transfer is dominated by these oscillations, and the contrast between the two regimes blurs out (figure 5).

In a recent set of ringdown experiments on silica bar micromechanical oscillators [13], and graphene drum nanomechanical oscillators [12], unusual regimes of energy dissipation were revealed, and explained in terms of the internal coupling of two oscillation modes. It is worthwhile mentioning that, although the discussion of these results was based on the energy exchange between the modes, the quantities accessible to experimental measurement were the oscillation amplitudes –typically, of one of the two modes. In one of the regimes, reported for both kinds of oscillator, the measured amplitude remained virtually constant for a sizable time interval (from 10 to 100 ms, depending on the experiment) after the external forcing was turned off. Only when this interval had elapsed, did the amplitude begin to decay, as expected due to damping. In another regime, observed in the graphene oscillator only, the amplitude exhibited a transition in the decay rate, with fast decay during the initial stage and a crossover to slower decay for longer times. Mathematical models were proposed in the form of equations of motion for two coupled oscillators –representing the oscillation modes–and the two regimes of energy dissipation were observed in their numerical solution. In both cases, the discussion emphasized the role of nonlinear mechanisms in controlling these phenomena.

On the light of the results of the present contribution, the regime in which the amplitude remains initially constant and then decays cannot be explained in terms of purely linear oscillations. In a linear combination of two decaying modes, in fact, it is not possible to have dominance of the slower mode for short times, and of the faster mode for long times. Obviously, if the slower mode is initially dominant, it can never be taken over by a faster decay. On the other hand, the regime where the amplitude decay changes from fast to slow can clearly occur in a system of two coupled linear oscillators. Indeed, we have found such behavior for the initial conditions leading to maximal total energy exchange, as shown in the leftmost panel of figure 3. Although we cannot discard that, in the experiments, nonlinear forces have a substantial effect on the overall dynamics, explaining the specific observation of crossover from fast to slow decay may not need to resort to nonlinearity. A more detailed, quantitative comparison between experiments and models should be necessary to decide on this issue.

Acknowledgments

The author thanks Daniel López and Changyao Chen for collaboration and enlightening discussions on the dynamics of micromechanical oscillators.

ORCID iDs

Damián H Zanette https://orcid.org/0000-0003-0681-0592

References

[1] Dincer I 2018 *Comprehensive Energy Systems* (Cambridge, MA: Elsevier)
[2] Wang H, Jasim A and Chen X 2018 Energy harvesting technologies in roadway and bridge for different applications–A comprehensive review *Appl. Energy* **212** 1083–94
[3] Vakakis A, Kerschen G, McFarland D, Gendelman O and Lee Y 2008 *Nonlinear Targeted Energy Transfer in Mechanical and Structural Systems* (Dordrecht: Springer)
[4] Okamoto H, Mahboob I, Onomitsu K and Yamaguchi H 2014 Rapid switching in high-Q mechanical resonators *Appl. Phys. Lett.* **105** 083114
[5] van Beek J and Puers R 2012 A review of MEMS oscillators for frequency reference and timing applications *J. Micromech. Microeng.* **22** 013001
[6] Abbott B *et al* (LIGO Scientic Collaboration and Virgo Collaboration) 2016 Observation of gravitational waves from a binary black hole merger *Phys. Rev. Lett.* **116** 061102
[7] Reinhardt C, Müller T, Bourassa A and Sankey J 2016 Ultralow-Noise SiN trampoline resonators for sensing and optomechanics *Phys. Rev.* X **6** 021001
[8] Schneider B, Singh V, Venstra W, Meerwaldt H and Steele G 2014 Observation of decoherence in a carbon nanotube mechanical resonator *Nat. Comm.* **5** 5819
[9] Chen C, Zanette D, Guest J, Czaplewski D and Lopez D 2016 Self-sustained micromechanical oscillator with linear feedback *Phys. Rev. Lett.* **117** 017203
[10] Polunin P, Yang Y, Dykman M, Kenny T and Shaw S 2016 Characterization of MEMS resonator nonlinearities using the ringdown response *J. MEMS* **25** 297–303
[11] Bhupathi P, Groszkowski P, DeFeo M, Ware M, Wilhelm F and Plourde B 2016 Transient dynamics of a superconducting nonlinear oscillator *Phys. Rev. Applied* **5** 024002
[12] Güttinger J, Noury A, Weber P, Eriksson A, Lagoin C, Moser J, Eichler C, Wallra A, Isacsson A and Bachtold A 2017 Energy-dependent path of dissipation in nanomechanical resonators *Nat. Nanotech.* **12** 631–6
[13] Chen C, Zanette D, Czaplewski D, Shaw D and López D 2017 Direct observation of coherent energy transfer in nonlinear micromechanical oscillators *Nat. Comm.* **8** 15523
[14] Lifshitz R and Cross M 2009 Nonlinear dynamics of nanomechanical and micromechanical resonators *Reviews of Nonlinear Dynamics and Complexity* vol 1 ed H Schuster (Weinheim: Wiley-VCH Verlag)
[15] Antonio D, Zanette D and López D 2012 Frequency stabilization in nonlinear micromechanical oscillators *Nat. Comm.* **3** 806
[16] Shoshani O, Shaw S and Dykman M 2017 Anomalous decay of nanomechanical modes going through nonlinear resonance *Sci. Rep.* **7** 18091
[17] Politzer D 2015 The plucked string: an example of non-normal dynamics *Am. J. Phys.* **83** 395–402
[18] Nayfeh A and Balachandran A 1989 Modal interactions in dynamical and structural systems *Appl. Mech. Rev.* **42** S175–201
[19] Nayfeh A and Mook D 1995 *Nonlinear Oscillations* (Hoboken, NJ: Wiley)
[20] Lomen D and Mark J 1986 *Ordinary Dierential equations with Linear Algebra* (Upper Saddle River, NJ: Prentice-Hall)
[21] José J and Saletan E 2013 *Classical Dynamics: A Contemporary Approach* (Cambridge: Cambridge University Press)
[22] Peng H, Chang C, Aloni S, Yuzvinsky T and Zettl A 2006 Ultrahigh frequency nanotube resonators *Phys. Rev. Lett.* **97** 087203
[23] Shaw A, Hill T, Neild S and Friswell M 2016 Periodic responses of a structure with 3:1 internal resonance *Mech. Syst. Signal Process.* **81** 19–34
[24] Perkins E 2017 Effects of noise on the frequency response of the monostable Duffing oscillator *Phys. Lett.* A **381** 1009–13
[25] Prigogine I 1968 *Introduction to Thermodynamics of Irreversible Processes* (Hoboken, NJ: Wiley)
[26] Martyushev L and Seleznev V 2006 Maximum entropy production principle in physics, chemistry and biology *Phys. Rep.* **426** 1–45